


## ORIGINAL ARTICLE

# Posterior Alpha and Gamma Oscillations Index Divergent and Superadditive Effects of Cognitive Interference

Alex I. Wiesman <sup>1,2</sup> and Tony W. Wilson<sup>1,2</sup><sup>1</sup>Department of Neurological Sciences, University of Nebraska Medical Center, Omaha, NE 68198-8440, USA and <sup>2</sup>Center for Magnetoencephalography, UNMC, Omaha, NE 68198-8440, USAAddress correspondence to Tony W. Wilson, Center for Magnetoencephalography, 988422 Nebraska Medical Center, Omaha, NE 68198-8422, USA.  
Email: twwilson@unmc.edu

## Abstract

Conflicts at various stages of cognition can cause interference effects on behavior. Two well-studied forms of cognitive interference are stimulus–stimulus (e.g., Flanker), where the conflict arises from incongruence between the task-relevant stimulus and simultaneously presented irrelevant stimulus information, and stimulus–response (e.g., Simon), where interference is the result of an incompatibility between the spatial location of the task-relevant stimulus and a prepotent motor mapping of the expected response. Despite substantial interest in the neural and behavioral underpinnings of cognitive interference, it remains uncertain how differing sources of cognitive conflict might interact, and the spectrally specific neural dynamics that index this phenomenon are poorly understood. Herein, we used an adapted version of the multisource interference task and magnetoencephalography to investigate the spectral, temporal, and spatial dynamics of conflict processing in healthy adults ( $N = 23$ ). We found a double-dissociation such that, in isolation, stimulus–stimulus interference was indexed by alpha (8–14 Hz), but not gamma-frequency (64–76 Hz) oscillations in the lateral occipital regions, while stimulus–response interference was indexed by gamma oscillations in nearby cortices, but not by alpha oscillations. Surprisingly, we also observed a superadditive effect of simultaneously presented interference types (multisource) on task performance and gamma oscillations in superior parietal cortex.

**Key words:** double dissociation, magnetoencephalography, multisource interference task, neural oscillations, superadditivity

## Introduction

The presence of irrelevant and/or conflicting stimuli generally has a negative impact on task performance, and these detrimental effects are broadly referred to as cognitive interference. The effects of this interference on behavior are well documented using a number of different paradigms and can be a result of conflicts at either the stimulus perception (i.e., stimulus–stimulus conflict) or response selection (i.e., stimulus–response conflict) stage. For instance, the presence of task-irrelevant distractor stimuli flanking the target stimulus has been found to interfere with efficient stimulus perception (Eriksen and Eriksen 1974), a phenomenon commonly referred to as the Eriksen

“Flanker” effect. In these experiments, the source of cognitive interference (i.e., the flanking stimuli) is external, and participants must rely on selective attention processes to mitigate the negative consequences of the distractors on performance. On the other hand, the prepotent mapping of basic motor responses has been found to interfere with task performance when the mapped responses are in conflict with the (task-irrelevant) spatial location of the target stimulus (Simon 1990); such interference is commonly termed the “Simon” effect.

Over the past 20 years, there has been a strong and sustained interest in identifying the neural circuitry that supports conflict processing in the human brain, and a number of functional

magnetic resonance imaging (fMRI) studies have documented network activation in the frontal, parietal, and occipital cortices (Peterson et al. 2002; van Veen and Carter 2002; Bush et al. 2003; Liu et al. 2004; Fröhholz et al. 2011). Specifically, the anterior cingulate has been implicated as a so-called “conflict monitor,” which signals other involved brain regions to the occurrence of unexpected and/or interfering events (van Veen and Carter 2002). In contrast, dorsolateral prefrontal regions are known to inhibit prepotent responses in the case of conflict (Aron et al. 2004, 2014) and adjust task-relevant behavior accordingly (Fox et al. 2006; He et al. 2007; Hampshire et al. 2010; Verbruggen et al. 2010; Wiesman et al. 2017). Parietal regions, and in particular, the superior parietal cortices are known to be essential in the mapping of spatial saliency, and the integration of this “map” with a task-relevant motor plan (Mountcastle et al. 1975; Lynch et al. 1977; Posner et al. 1984; Corbetta et al. 1995; Colby and Goldberg 1999; Desmurget et al. 1999; Yantis et al. 2002; Buschman and Miller 2007; He et al. 2007; Van Der Werf et al. 2008; Capotosto et al. 2009; Bisley and Goldberg 2010). Finally, more recent research has established that neural responses in tertiary visual areas are influenced by cognitive interference (McDermott et al. 2017; Janssens et al. 2018), signaling an attentional enhancement of bottom-up information. Although the spatial aspects of these networks are well known, far fewer studies have focused on their spectrotemporal dynamics, and even fewer have attempted to delineate the unique effects of different sources of cognitive interference (e.g., Simon vs. Flanker effects) on the neural dynamics.

Differing frequencies of oscillatory neural responses have been found to be essential for the coding of particular cognitive functions, including the mitigation of cognitive interference (Hanslmayr et al. 2008; Wiesman and Wilson 2019; Wiesman et al. 2019; Gulbinaite et al. 2017; McDermott et al. 2017; Janssens et al. 2018), and these responses often occur on a subsecond timescale. For instance, transient decreases in the power of alpha-frequency oscillations in the posterior parietal-occipital cortices have been previously found to index stimulus–stimulus interference on a variety of cognitive tasks (West and Bell 1997; Hanslmayr et al. 2008; Ergen et al. 2014; Nombela et al. 2014; McDermott et al. 2017; Janssens et al. 2018; Suzuki et al. 2018). Perhaps surprisingly, very few studies have investigated the effect of cognitive interference on gamma-frequency oscillations, which have been extensively linked to the processing and prioritizing of visual stimulus information (Gruber et al. 1999; Shibata et al. 1999; Tallon-Baudry and Bertrand 1999; Bertrand and Tallon-Baudry 2000; Başar et al. 2001; Busch et al. 2004; Tallon-Baudry et al. 2005; Vidal et al. 2006; Womelsdorf et al. 2006; Jensen et al. 2007, 2014; Siegel et al. 2007; Doesburg et al. 2008; Edden et al. 2009; Koelewijn et al. 2013; Muthukumaraswamy and Singh 2013; Landau et al. 2015; Marshall et al. 2015; Wiesman et al. 2017, 2018a), as well as the integration of this stimulus information with saliency mapping and motor planning (Pesaran et al. 2002; Womelsdorf et al. 2006; Womelsdorf and Fries 2006; Van Der Werf et al. 2008). Thus, it remains essential to investigate the neural bases of differing subtypes of cognitive interference using methodologies with sufficient temporal precision to capture not only the rapid and transient nature of these responses, but also their spectral dynamics (i.e., their unique frequency composition). In a notable step toward this goal, one group (Wang et al. 2014) used a combined Simon–Stroop task and electroencephalography to tease apart the time course and spectral dynamics of neural responses to stimulus–stimulus and stimulus–response cognitive interference. They

showed that both alpha- and beta-band activities were critical to the processing of cognitive interference, but were unable to delineate the cortical origins of these frequency-dependent effects and did not examine gamma-frequency activity.

This study aims to fill two major gaps in the cognitive neuroscience literature. First, how do neural responses to stimulus–stimulus and stimulus–response subtypes of cognitive interference differ in time, space, and frequency? Second, how do these forms of cognitive interference affect high-frequency neural activity in the gamma band? To answer these questions, we utilize the unique spatial and temporal precision of magnetoencephalography (MEG), combined with a novel adaptation of the multisource interference task (MSIT; Bush et al. 2003; Bush and Shin 2006) to characterize the neural dynamics underlying divergent and convergent effects of stimulus–stimulus (Flanker) and stimulus–response (Simon) cognitive interference. Twenty-three healthy young adult participants performed the task, and significant oscillatory responses were imaged using a beamformer. Whole-brain statistical comparisons were used to examine the effect of interference condition on transient, frequency-specific neural responses. Our hypotheses were twofold. First, based on earlier research using flanker tasks (McDermott et al. 2017, 2019; Janssens et al. 2018; Suzuki et al. 2018), we expected that alpha-frequency oscillations in the lateral occipital cortex would increase (i.e., stronger event-related desynchronization responses) as a function of stimulus–stimulus interference. Second, despite the lack of previous research into the effects of cognitive interference on gamma oscillations, we hypothesized that such high-frequency responses would scale with stimulus–response interference in lateral occipital and superior parietal cortex. This hypothesis was based on the existing literature supporting the integral nature of posterior gamma oscillations in the mapping of visual saliency and the synthesis of task-relevant motor plans.

By focusing not only on the spatial origins of these dynamics, but also on their temporal and spectral properties, we provide novel evidence for a double dissociation of interference subtypes in the lateral occipital cortices by oscillatory frequency. Specifically, as was hypothesized, we find that alpha-frequency oscillations in the right lateral occipital cortices preferentially support the processing of Flanker interference effects, while gamma-frequency oscillations in nearby regions preferentially process Simon interference effects. Furthermore, and surprisingly, we note a striking superadditive effect of cognitive interference subtypes on performance (i.e., reaction time [RT] and accuracy). After investigating this effect further, we find that gamma oscillatory responses in the left parieto-occipital cortices also index this superadditivity and are significantly related to task performance. Conceptually, superadditivity effects represent the inefficient sharing of neural resources by competing cognitive processes. For example, presenting an auditory and visual stimulus together often elicits more neural spikes than presenting each in isolation, and there are other classic examples in the neurophysiological literature (Holmes and Spence 2005). In sum, herein, we find both divergent and convergent indexing of cognitive interference by distinct spatio-spectral patterns of neural activity.

## Materials and Methods

### Participants

Twenty-three healthy young adults were recruited for the study ( $M_{\text{age}} = 26.09$ ; age range: 20–33 years; 16 males; 21 right handed).

Exclusion criteria included any medical illness affecting central nervous system function, any neurological or psychiatric disorder, history of head trauma, current substance abuse, and any nonremovable metal implants that would adversely affect MEG data acquisition. All participants had normal or corrected-to-normal vision. The Institutional Review Board at the University of Nebraska Medical Center reviewed and approved this investigation. Written informed consent was obtained from each participant following detailed description of the study, and all study protocols conformed to the Declaration of Helsinki. All participants completed the same experimental protocol.

### MEG Experimental Paradigm and Behavioral Data Analysis

We used a modified version of the MSIT (Bush et al. 2003; Bush and Shin 2006) to engage cognitive interference networks (Fig. 1). Each trial began with a central fixation presented for a randomly varied interstimulus interval of 2000–2400 ms. The fixation was then replaced by a vertically centered horizontal row of three equally spaced integers between 0 and 3. These integer stimuli were presented for 1500 ms. Two of these numbers were always identical (task irrelevant) and the third different (task relevant). Prior to beginning the experiment, participants were given a right-handed five-finger button pad and instructed that the index, middle, and ring finger locations represented the integers 1, 2, and 3, respectively. Participants were then instructed that on each trial, they would be presented with a horizontal row of three integers, and that the objective was to indicate the “odd-number-out” by pressing the button corresponding to its numerical identity (and not its spatial location). Speed and accuracy were also stressed to the participant at this point. Left-handed participants were required to use their right hand for this task, and exploratory analyses found behavioral patterns in these participants to be largely consistent with those exhibited by the larger dataset. Using these stimuli, four interference conditions were possible: (1) control (no interference; i.e., 1 0 0/0 2 0/0 0 3), (2) Simon (stimulus–response interference; i.e., 0 1 0/0 0 1/2 0 0/0 0 2/0 3 0/3 0 0), (3) Flanker (stimulus–stimulus interference; i.e., 1 2 2/1 3 3/1 2 1/3 2 3/1 1 3/2 2 3), and (4) multisource (both stimulus–response and stimulus–stimulus interference; i.e., 2 1 2/3 1 3/2 2 1/3 3 1/2 1 1/2 3 3/1 1 2/3 3 2/1 3 1/2 3 2/3 1 1/3 2 2). Trial types and responses were pseudorandomized over the course of the experiment, such that no interference condition nor any response was repeated more than twice in a row. Participants completed 100 trials of each interference condition, for a grand total of 400 trials, and a total recording time of ~24 min. Custom visual stimuli were programmed in Matlab (Mathworks, Inc.) using “Psychophysics Toolbox Version 3” (Brainard 1997) and back-projected onto a nonmagnetic screen. For each participant, accuracy data were computed as a percentage (correct/total trials). RT data were also extracted for each individual trial and incorrect and no-response trials were removed. Initial analyses suggested that no responses fell in time periods that were either physiologically implausible (i.e., faster than 150 ms) nor outside of the presentation of the target stimuli (i.e., slower than 1500 ms), and thus, no outliers were excluded at the single-trial level on the basis of behavior. Importantly, exploratory analyses confirmed that all of the significant behavioral effects reported in this manuscript also survived using a standard single-trial RT threshold of  $\pm 2.5$  standard deviations (SDs) from the mean. Measures of central tendency were then computed for single-trial RT data for each participant and condition, including the

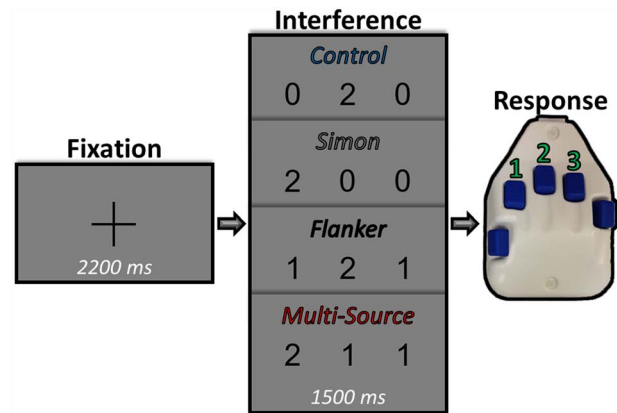


**Figure 1.** Experimental paradigm. Each trial began with a central fixation presented for a randomly varied interstimulus interval of 2000–2400 ms. After this, the fixation was replaced by a vertically centered horizontal row of three equally spaced integers between 0 and 3. The presentation of the integer stimuli lasted for 1500 ms. Two of these integers were always identical (task irrelevant) and the third was different (task relevant). Prior to beginning the experiment, participants were given a five-finger button pad and instructed that the index, middle, and ring finger locations represented the integers 1, 2, and 3, respectively. Participants were then instructed that on each trial they would be presented with a horizontal row of three integers, and that the objective was to indicate the “odd-number-out” by pressing the button corresponding to its numerical identity (and not its spatial location). Using these stimuli, four interference conditions were possible: (1) control (no interference), (2) Simon (stimulus–response interference), (3) Flanker (stimulus–stimulus interference), and (4) multisource.

harmonic mean for statistical analysis, as well as the simple mean for subsequent visualization and interpretation purposes. Briefly, the harmonic mean was used rather than the simple mean for statistical analysis, as this metric has been found to be a less-biased indicator of population RT data (Baayen and Milin 2010). Accuracy (in percent of trials answered correctly) was also computed, and the condition-wise distributions of both RT and accuracy data were tested for non-normality using the Shapiro–Wilk test. These tests did not suggest non-normality for any of the harmonic RT data (all  $P$ 's > 0.30), and thus a traditional repeated measures–analysis of variance (RM–ANOVA) was appropriate to test for condition effects in these data. In contrast, accuracy was non-normally distributed for all conditions (all  $P$ 's < 0.01). Thus, a nonparametric equivalent of the traditional RM–ANOVA, Friedman's test, was used instead.

RT and accuracy were analyzed for a main effect of interference condition using a four-way RM–ANOVA and Friedman's test, respectively, with interference condition as the only (within-subjects) factor of interest. Behavioral analyses were implemented in JASP (2018), an open-source statistical software. The ANOVA for RT was tested for violations of sphericity using Mauchly's test, and corrected using Greenhouse–Geisser correction. Friedman's test does not assume sphericity nor normality, and thus no such correction was necessary for the accuracy data. Follow-up tests for conditional differences were conducted using traditional paired-samples  $t$ -tests for the RT data and Conover's posthoc tests for the accuracy data, and were corrected for multiple comparisons using the Holm–Bonferroni method. We next performed targeted analysis to examine the potential for superadditive effects of multisource cognitive interference on behavior. To this end, we first computed the “interference effect” of each interference condition within each participant (i.e., the Flanker, Simon, and multisource conditions)

by subtracting each behavioral metric in the control condition from the same metric in each interference condition (e.g., Simon RT–control RT). From this, we were left with participant-level accuracy and RT values representing the difference in task performance caused by each type of interference. Again, we tested these models for normality prior to statistical testing using the Shapiro–Wilk test and found that the accuracy data, and not the harmonic RT data, exhibited significant deviations from normality. Thus, to test for superadditivity, we computed paired-samples' *t*-tests for RT and Wilcoxon signed-rank tests for accuracy, between the multisource interference condition and the summed effects of interference from the Simon and Flanker conditions, within each participant. Using these tests, a rejection of the null hypothesis would indicate that the simultaneous presentation of two interference types (multisource) affects task performance at a different magnitude than what would be expected by an additive model (Simon + Flanker).

### MEG Data Acquisition

All recordings were conducted in a one-layer magnetically shielded room with active shielding engaged for environmental noise compensation. Neuromagnetic responses were sampled continuously at 1 kHz with an acquisition bandwidth of 0.1–330 Hz using a 306-sensor Elekta MEG system (Helsinki, Finland) equipped with 204 planar gradiometers and 102 magnetometers. It is important to note that we only considered data from the planar gradiometers for this study. Participants were monitored during data acquisition via real-time audio–video feeds from inside the shielded room. Each MEG dataset was individually corrected for head motion and subjected to noise reduction using the signal space separation method with a temporal extension (Taulu and Simola 2006).

### Structural MRI Processing and MEG Coregistration

Preceding MEG measurement, four coils were attached to the participant's head and localized, together with the three fiducial points and scalp surface, using a 3D digitizer (Fastrak 3SF0002, Polhemus Navigator Sciences). Once the participant was positioned for MEG recording, an electric current with a unique frequency label (e.g., 322 Hz) was fed to each of the coils. The magnetic fields associated with these currents were then localized in reference to the sensors throughout the recording session. Since coil locations were also known in head coordinates, all MEG measurements could be transformed into a common coordinate system. With this coordinate system, each participant's MEG data were coregistered with individual structural T1-weighted MRI data ( $N = 13$ ), when available, or alternatively were fitted to a template MRI ( $N = 10$ ) using the scalp surface points, in BESA MRI (Version 2.0) prior to source space analysis. Importantly, these two approaches have been shown to yield very similar results (Holliday et al. 2003). Furthermore, none of our key neural metrics (i.e., the right occipital responses from the RM-ANOVAs and the left superior parietal response from the superadditivity analysis) significantly differed according to whether a template or individual MRI was used ( $P > 0.15$ ). All of our relevant statistical contrasts were also within subjects, which further mitigates concerns about any of our results being driven by a systematic bias between these methods. Structural MRI data were aligned parallel to the anterior and posterior commissures and transformed into standardized space. Following source analysis (i.e., beamforming), each participant's  $4.0 \times 4.0 \times 4.0$ -mm functional

images were also transformed into standardized space using the transform that was previously applied to the structural MRI volume and spatially resampled.

### MEG Preprocessing, Time–Frequency Transformation, and Sensor-Level Statistics

Cardiac and blink artifacts were identified in the raw recordings using the MEG sensors with the best signal-to-noise ratio (SNR) for the specific source of interference (i.e., near the orbits for eye blinks/movements and near the inferior temporal cortices for cardiac events) and removed from the data using signal space projection (SSP), which was subsequently accounted for during source reconstruction (Uusitalo and Ilmoniemi 1997). The continuous magnetic time series was then divided into 1500-ms epochs, with the baseline extending from -500 to 0 ms prior to the onset of the probe stimuli. Epochs containing remaining artifacts (after SSP) were rejected per participant using a fixed threshold method, supplemented with visual inspection. An average amplitude threshold of 1009.78 (SD = 169.18) fT and an average gradient threshold of 226.81 (SD = 89.86) fT/s was used to reject artifacts. Across the group, an average of 338.09 (SD = 11.15) trials per participant were used for further analysis. The number of accepted trials did not differ across the four cognitive interference conditions ( $P > 0.50$ ), which was essential, as our primary analyses consisted of statistical comparisons between these conditions and could have been biased by conditional differences in the SNR.

The artifact-free epochs (-500 to 1000 ms, with zero defined as visual stimulus onset) were next transformed into the time–frequency domain using complex demodulation (Kovach and Gander 2016) with a time/frequency resolution of 2 Hz/25 ms and a bandwidth of 4–100 Hz. The resulting spectral power estimations per sensor were then averaged over trials to generate time–frequency plots of mean spectral density. These sensor-level data were normalized by each respective frequency bin's baseline power, which was calculated as the mean power during the -500 to 0 ms of time period. The specific time–frequency windows used for subsequent source imaging were determined by statistical analysis of the sensor-level spectrograms across all conditions and the entire array of gradiometers. Each data point in the spectrogram was initially evaluated using a mass univariate approach based on the general linear model. To reduce the risk of false-positive results while maintaining reasonable sensitivity, a two-stage procedure was followed to control type 1 error. In the first stage, paired-sample *t*-tests against baseline were conducted on each data point and the output spectrogram of *t*-values was thresholded at  $P < 0.05$  to define time–frequency bins containing potentially significant oscillatory deviations across all participants. In stage two, the time–frequency bins that survived the threshold were clustered with temporally and/or spectrally neighboring bins that were also below the threshold ( $P < 0.05$ ), and a cluster value was derived by summing all of the *t*-values of all data points in the cluster. Nonparametric permutation testing was then used to derive a distribution of cluster values, and the significance level of the observed clusters (from stage one) were tested directly using this distribution (Ernst 2004; Maris and Oostenveld 2007). For each comparison, 1000 permutations were computed to build a distribution of cluster values. Based on these analyses, the time–frequency windows that contained significant oscillatory events across all participants were subjected to a beamforming analysis. This approach was taken



for two primary reasons: (1) by defining our time–frequency bins using a data-driven method, we remove a level of subjectivity from our analysis (and thus enhance replicability for future studies) and (2) by only performing subsequent analyses on time–frequency windows that exhibited a significant change from prestimulus baseline periods, we enhance the SNR of our data, thereby increasing the confidence in the robustness of our measured neural responses. Importantly, the distribution of our trial numbers ensures that this sensor-level selection analysis can be reasonably assumed to be orthogonal to subsequent tests for condition-wise differences and superadditivity, mitigating any concerns regarding circularity (Kriegeskorte et al. 2009).

### MEG Source Imaging

Cortical networks were imaged through an extension of the linearly constrained minimum variance vector beamformer known as dynamic imaging of coherent sources (Gross et al. 2001), which applies spatial filters to time–frequency sensor data in order to calculate voxel-wise source power for the entire brain volume. Imaging of oscillatory responses was performed per condition, per participant for the statistically defined time–frequency bins in the alpha (8–14 Hz; 300–600 ms), beta (18–28 Hz; 350–750 ms), and gamma [(64–76 Hz; 150–400 ms) and (68–80 Hz; 475–700 ms)] bands. Further information is provided in the Results section. The single images were derived from the cross-spectral densities of all combinations of MEG gradiometers averaged over the time–frequency range of interest, and the solution of the forward problem for each location on a grid specified by input voxel space. Following convention, we computed noise-normalized, source power per voxel in each participant using active (i.e., task) and passive (i.e., baseline) periods of equal duration and bandwidth. Such images are typically referred to as pseudo-t maps, with units (pseudo-t) that reflect noise-normalized power differences (i.e., active vs. passive) per voxel. This generated participant-level pseudo-t maps for each time–frequency-specific response identified in the sensor-level cluster-based permutation analysis. MEG preprocessing and imaging used the Brain Electrical Source Analysis (BESA version 6.1) software.

### MEG Source Statistics

To initially investigate the spatial location of each frequency-specific neural response to the task, we computed grand-average maps per time–frequency response, collapsing across all interference conditions. For this analysis, we imaged the data in each participant using all trials within each statistically defined time–frequency response window regardless of cognitive interference condition, and averaged these participant-wise maps to create one grand-averaged map per oscillatory response for the entire group. These grand-average maps were used to discern the nature of each response (e.g., motor vs. visual) and target subsequent analyses toward responses originating from nonmotor regions, as investigating somato-motor processing of cognitive interference was not an aim of this study. For example, we did not further investigate the beta or later gamma response because the grand-average maps suggested exclusively somato-motor processing in these time–frequency windows.

To examine interference-related differences in frequency-specific neural activity, we conducted RM-ANOVAs in SPM12 for each time–frequency response of interest (alpha and early gamma) using the voxel-wise data across the entire brain.

Significant clusters were identified using a relatively strict initial threshold of  $P < 0.005$ , followed by a cluster-size correction of  $k > 500$  contiguous voxels, based on the theory of Gaussian random fields (Poline et al. 1995; Worsley et al. 1996, 1999). From the resulting significant clusters, pseudo-t values per participant were extracted from the peak voxel (i.e., the voxel with the highest value per cluster), and these were used in posthoc testing. Of note, this method of extracting representative data from the peak voxel, rather than the average across a mask defined region or similar method, is not without limitations. However, this approach does avoid some amount of arbitrariness, as it identifies the data of interest without selecting a mask a priori, and represents the most robust effects. On the other hand, this approach requires a level of extrapolation to infer that these data represent the same pattern of effects across the significant cluster from which they were extracted. Posthoc testing consisted of checks for sphericity violations using Mauchly's test, and if necessary computation of Greenhouse–Geisser corrected  $P$  values. Importantly, none of our significant tests became nonsignificant when applying this correction. All posthoc  $t$ -tests were also corrected for multiple comparisons using the Holm–Bonferroni method (i.e., corrected for the comparisons made within the respective model—six posthoc tests per model), and the results of this correction are indicated in [Supplementary Figure 1](#). To also qualitatively examine the temporal evolution of these responses per condition, we computed virtual sensor data by applying the sensor-weighting matrix derived through the forward computation to the preprocessed signal vector, which yielded a time series derived from the location of interest. These data were then decomposed into the time–frequency domain, averaged over the relevant frequency band of interest, and are displayed in [Supplementary Figures 2–4](#).

Finally, we computed whole-brain statistical maps investigating the potential for superadditivity of multisource interference on the neural dynamics, similar to the comparisons made to test for superadditivity in the behavioral metrics. For this analysis, we first performed a voxel-wise subtraction of the control condition map from each of the three interference condition maps for each participant per time–frequency component (i.e., alpha and early gamma). This produced participant-level whole-brain interference effect maps for each of the Simon, Flanker, and multisource conditions. We then summed the voxel-wise values of the Simon and Flanker interference effect maps to produce a whole-brain map (per participant, per neural response), which represented the null hypothesis of an additive model. To then test the potential for superadditivity statistically, whole-brain paired-samples  $t$ -tests were computed between the multisource interference model maps and these additive-model maps. It is important to note that these tests were performed one-tailed, since a two-tailed test would also investigate significant subadditive effects, and such an analysis was not justified by the behavioral data and would be inherently difficult to interpret. Furthermore, it should also be stressed that these tests for superadditivity were motivated entirely posthoc after initial analysis of our behavioral data, and that superadditivity analyses were not an original hypothesis of this study. The end result of this analysis was two spectrally defined (i.e., one alpha and one gamma) whole-brain statistical maps showing the cortical regions that exhibited a significantly larger interference effect in the multisource condition than what would be expected from the additive model ( $H_1$ : multisource > Simon + Flanker).

**Table 1** Central tendency and variability of behavior by condition.

	Condition	Mean (SD)	Median (MAD)
RT (ms)	Control	653.15 (111.10)	664.52 (70.10)
	Simon	717.77 (120.89)	685.40 (73.49)
	Flanker	770.26 (116.15)	782.42 (87.43)
	Multisource	865.91 (121.85)	864.54 (107.85)
Accuracy (% correct)	Control	98.42 (1.42)	98.98 (0.03)
	Simon	95.86 (3.28)	96.97 (1.92)
	Flanker	97.96 (2.13)	97.98 (1.02)
	Multisource	93.68 (4.28)	95.83 (2.08)

MAD, median absolute deviation.

Once again, pseudo-*t* values per participant were extracted from the peak voxel of each cluster in these maps for further testing. These data were also tested for normality using the Shapiro–Wilk method, and in cases where either of the variables was significantly non-normal, a comparable nonparametric test was used (e.g., a Spearman's rank order coefficient rather than a Pearson's coefficient). To again account for multiple comparisons, an initial significance threshold of  $P < 0.005$  was used for the identification of significant clusters in these whole-brain statistical maps, accompanied with a cluster (*k*) threshold of at least 500 contiguous voxels.

## Results

### Effects of Cognitive Interference on Task Performance

Overall, participants performed well on the task (Fig. 1), with a mean accuracy of 96.49% (SD=2.29%) and a mean RT of 749.97 ms (SD=114.56 ms). Condition-wise behavioral data can be found in Table 1. RM tests for conditional effects (Fig. 2) revealed a significant effect of interference condition on both accuracy (Friedman's test;  $\chi^2(3, N = 23) = 43.57, P < 0.001$ ) and RT (RM-ANOVA;  $F(2.36, 51.82) = 253.27, P < 0.001$ ). Participants were significantly slower to respond on the Simon (paired *t*-test;  $t(22) = 9.69, P < 0.001$ ), Flanker (paired *t*-test;  $t(22) = 15.68, P < 0.001$ ), and multisource (paired *t*-test;  $t(22) = 22.84, P < 0.001$ ) trials relative to the control trials. Furthermore, participants were significantly slower in the multisource condition than both the Simon (paired *t*-test;  $t(22) = 19.29, P < 0.001$ ) and Flanker (paired *t*-test;  $t(22) = 14.26, P < 0.001$ ) conditions. Participants also responded significantly slower on Flanker than Simon trials (paired *t*-test;  $t(22) = 5.02, P < 0.001$ ). The results of the posthoc comparisons for accuracy were generally similar to the RT results. Posthoc comparisons for accuracy revealed that participants were significantly less accurate in the Simon (Conover's test;  $t(69) = -4.27, P < 0.001$ ) and multisource (Conover's test;  $t(69) = -5.79, P < 0.001$ ) conditions than in the control condition. Furthermore, participants were significantly less accurate in the multisource condition than in the Flanker condition (Conover's test;  $t(69) = -4.61, P < 0.001$ ). Finally, participants were less accurate in the Simon condition than in the Flanker condition (Conover's test;  $t(69) = -3.09, P = 0.009$ ). No significant differences in accuracy were found between control and Flanker conditions nor between the Simon and multisource conditions. All behavioral posthoc results remained significant after correction for multiple comparisons.

Upon visual inspection of these data, it became apparent that a superadditive effect of MSIT performance was possible. Indeed, statistical tests between the effect of multisource interference and the additive model (Simon interference + Flanker interference) were significant for RT (paired *t*-test;  $t(22) = -5.32, P < 0.001$ ) and trending for accuracy (Wilcoxon signed-rank test;  $Z(N = 23) = 82, P = 0.092$ ), such that the concurrent presentation of the two interference sources worsened the behavior, as compared to their additive effects in isolation.

### Spectral, Temporal, and Spatial Definitions of Neural Responses to the Task

Before testing the MEG measures for a main effect of interference condition, we first had to determine the time–frequency windows containing major neural responses across the four conditions. After transforming the data into time–frequency space, we observed robust activity in the alpha, beta, and gamma bands (Fig. 3). Specifically, an early desynchronization in the alpha (8–14 Hz; 300–600 ms) band across parieto-occipital sensors coincided temporally with a much higher frequency synchronization in the gamma (64–76 Hz; 150–400 ms) band in posterior occipital sensors. Occurring slightly later were two responses in the beta (18–28 Hz; 350–750 ms) and gamma (68–80 Hz, 475–700 ms) bands, both of which were centered in the left somato-motor sensors. Source imaging of these responses revealed that the early alpha and gamma responses were originating bilaterally from lateral occipital and primary visual regions, respectively. In contrast, the later beta and gamma responses were both found to originate from the hand-knob region of the precentral gyrus, implicating them in the processing of the motor response. As investigating somato-motor processing of cognitive conflict was not an aim of this study, these responses were not examined in subsequent whole-brain statistical analyses.

### Alpha and Gamma Oscillations Index Divergent and Superadditive Effects of Cognitive Interference

To examine the neural dynamics underlying the three types of cognitive interference, we used the condition-specific participant-level maps to compute whole-brain RM-ANOVAs for the visual alpha and gamma responses. For these statistical comparisons, the within-subjects factor of interference condition was of interest. In the alpha range, a robust main effect of condition was observed in the right lateral occipital ( $F(3,66) = 7.06, P < 0.001$ ) and right cerebellar ( $F(3,66) = 7.30, P < 0.001$ ) regions (Fig. 4). Posthoc testing revealed that alpha activity in the right lateral occipital distinguished the control and Simon conditions from the Flanker and multisource conditions, such that the decrease from baseline was greater than in the control condition for Flanker ( $t(22) = -3.89, P < 0.001$ ) and multisource ( $t(22) = -2.98, P = 0.007$ ) interference, but not for Simon ( $t(22) = -0.09, P = 0.926$ ) interference. The magnitude of the alpha decrease was also greater for Flanker interference than for Simon interference ( $t(22) = -3.68, P = 0.001$ ), and no significant difference in the alpha response was observed between Flanker and multisource interference ( $t(22) = 0.23, P = 0.820$ ). Finally, the alpha response was significantly larger for multisource than for Simon interference ( $t(22) = -2.63, P = 0.015$ ). Importantly, all of these effects remained significant following correction for multiple comparisons. Alpha activity in the right cerebellum exhibited the same distinction between Simon and

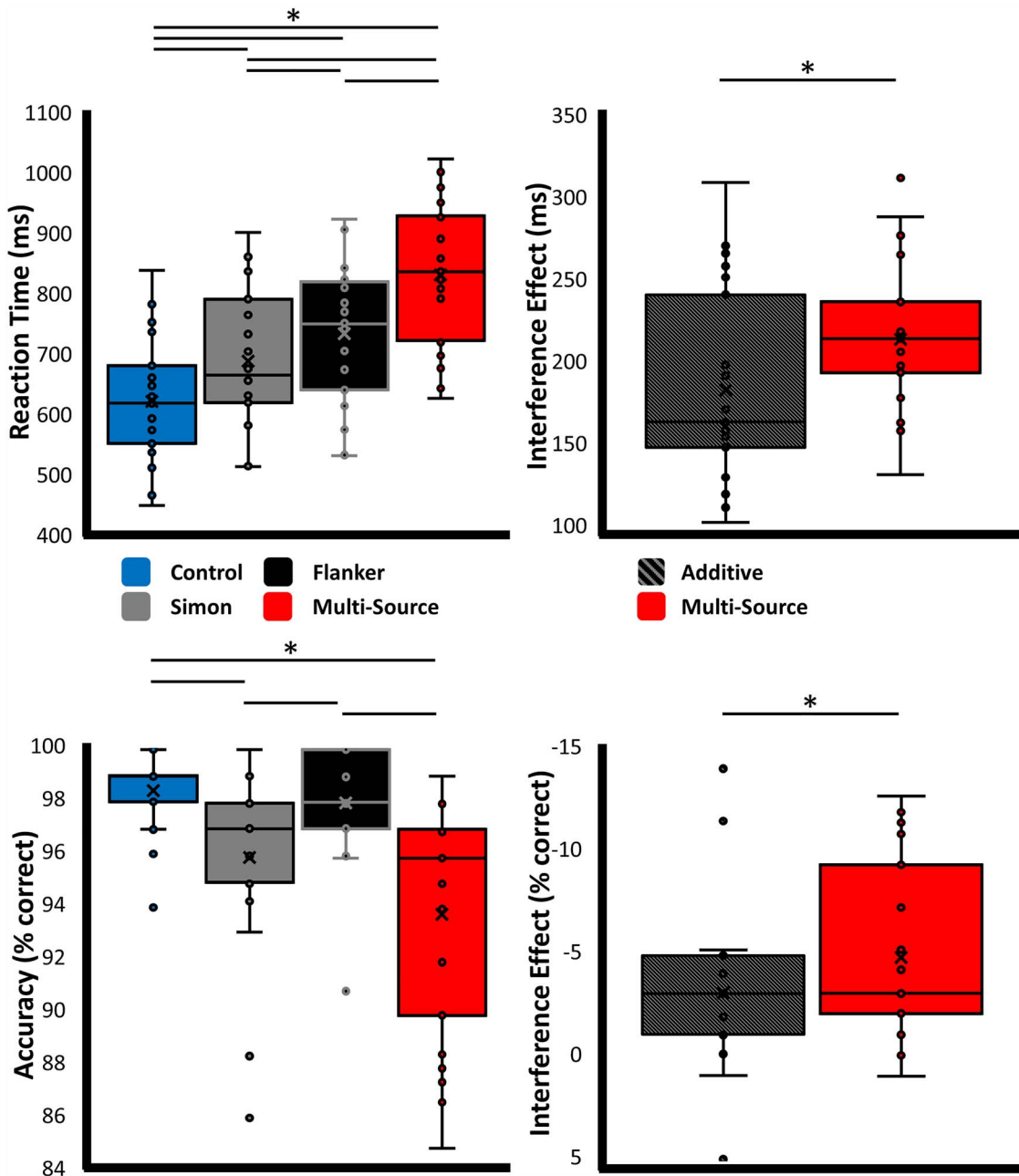


**Figure 2.** Behavioral results. Results from the behavioral analyses, with data for the main effect of interference condition presented on the left, and results from the superadditivity analyses on the right. Plots display the individual data points, along with the median (horizontal line), mean (x), first and third quartile (box), and local minima and maxima (whiskers). \* $P < 0.01$ , corrected.

Flanker interference, with a similar pattern of significance (see [Supplementary Table 1](#) for comprehensive posthoc results).

A similar whole-brain RM-ANOVA for the visual gamma response also revealed a robust main effect of interference type in the right lateral occipital cortex ( $F(3,66) = 6.06$ ,  $P = 0.001$ ; [Fig. 5](#)). In contrast to the alpha response in right lateral occipital cortex, which distinguished control and Simon interference from Flanker and multisource, the gamma response in the same general region instead distinguished control and Flanker interference from Simon and multisource interference. Posthoc testing showed that the gamma increase from baseline was

greater than in the control condition for Simon ( $t(22) = 2.88$ ,  $P = 0.009$ ) and multisource ( $t(22) = 2.86$ ,  $P = 0.009$ ) interference, but not Flanker ( $t(22) = -0.13$ ,  $P = 0.897$ ) interference ([Fig. 5](#)). The magnitude of this gamma increase was also greater for Simon interference than for Flanker interference ( $t(22) = 3.33$ ,  $P = 0.003$ ), and no significant difference in the gamma response was observed between Simon and multisource interference ( $t(22) = -0.21$ ,  $P = 0.834$ ). Finally, the gamma response was significantly larger for multisource than for Flanker interference ( $t(22) = 2.81$ ,  $P = 0.01$ ). Again, all of these effects remained significant after correcting for multiple comparisons. For

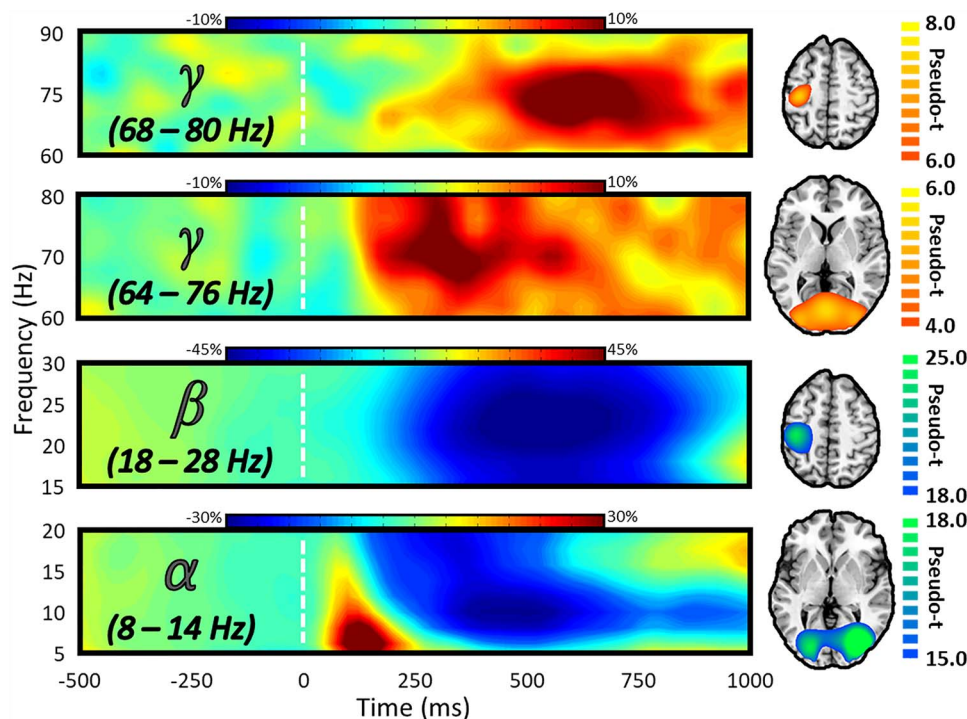


**Figure 3.** Spectral, temporal, and spatial definitions of neural responses to the MSIT task. The MEG sensor spectrograms (left) display the time–frequency representations of neural responses identified by cluster-based permutation analysis (see section Methods). Time (in ms) is denoted on the x-axis and frequency (in Hz) is denoted on the y-axis, and the dashed white line at 0 ms indicates the onset of the integer stimuli. The color scale bar for percent change from baseline is displayed above each plot. Each spectrogram represents group-averaged data from one gradiometer sensor that was representative of the neural responses in sensors over either occipito-parietal (second and fourth from the top) or somato-motor (first and third from the top) regions. On the far right is the source-imaged representation of each response, with the color scale bar to the right denoting response amplitude in pseudo-t units.

enhanced interpretation, peak-voxel time series visualizations of these condition-wise effects are also available for the alpha (Supplementary Figs 2 and 3) and gamma (Supplementary Fig. 4) responses.

Motivated by the superadditive effect observed in the behavioral data, we next performed a more targeted analysis to examine the potential for superadditive effects of cognitive interference subtypes on whole-brain oscillations. This analysis (see section “Materials and Methods: MEG Source Imaging and Statistics”) revealed a significant peak in the left superior parietal cortex in the gamma band, as well as in the right cerebellum (Fig. 6). Furthermore, the response superadditivity in the left superior parietal cortex (multisource interference/additive interference) covaried significantly with both measures of task performance (Spearman rank-order correlations; accuracy:  $r = -0.51$ ,  $P = 0.014$ ; RT:  $r = 0.52$ ,  $P = 0.011$ ), such that as response superadditivity increased, task performance decreased. Similar relationships with behavior were not present with response superadditivity in the right cerebellum (Spearman rank-order correlations; accuracy:  $r = -0.17$ ,  $P = 0.443$ ; RT:  $r = 0.24$ ,  $P = 0.277$ ). No significant superadditive effects were found in the alpha band.

## Discussion

By combining a novel adaptation of the MSIT, advanced source imaging of MEG data, and whole-brain statistical analyses, we identified the neural signatures of stimulus–stimulus and stimulus–response cognitive interference and discerned oscillatory responses in the posterior cortices that distinguish between

the two interference subtypes. Alpha-band power in the lateral occipital cortices has repeatedly been linked to visual attention and perception (Worden et al. 2000; Rihs et al. 2007; Capotosto et al. 2009; Foxe and Snyder 2011; Handel et al. 2011; Rohenkohl and Nobre 2011; Klimesch 2012; May et al. 2012; Herring et al. 2015; Marshall et al. 2015; Doesburg et al. 2016; Gulbinaite et al. 2017; McDermott et al. 2017; Wiesman et al. 2017, 2018b; Janssens et al. 2018), and is thought to index a form of active cortical inhibition (Kelly et al. 2006; van Dijk et al. 2008; Jensen and Mazaheri 2010; Romei et al. 2010; Handel et al. 2011; Bonnefond and Jensen 2012; Klimesch 2012; de Graaf et al. 2013; Jensen et al. 2014; Spaak et al. 2014; Heinrichs-Graham and Wilson 2015; Wiesman et al. 2016). Meanwhile, gamma-frequency activity in occipital regions is also modulated by attention (Gruber et al. 1999; Shibata et al. 1999; Tallon-Baudry et al. 2005; Vidal et al. 2006; Jensen et al. 2007; Doesburg et al. 2008; Marshall et al. 2015), but these rhythms have been convincingly tied to more fine-grained coding of stimulus features and object representation, such as complexity, size, and duration (Tallon-Baudry and Bertrand 1999; Bertrand and Tallon-Baudry 2000; Posada et al. 2003; Busch et al. 2004; Muthukumaraswamy and Singh 2013). Furthermore, visual and posterior parietal gamma activities has been proposed as an early neural correlate of efficient visuo-motor integration (Pesaran et al. 2002; Womelsdorf et al. 2006; Womelsdorf and Fries 2006; Van Der Werf et al. 2008). At the cell-circuit level, high-frequency gamma oscillations are known to be the result of a dynamic balance between local excitatory (e.g., glutamatergic pyramidal) and inhibitory (e.g., GABAergic interneuron) cells (Edden et al. 2009; Muthukumaraswamy et al. 2009; Tiesinga and Sejnowski 2009; Gaetz et al. 2011; Uhlhaas



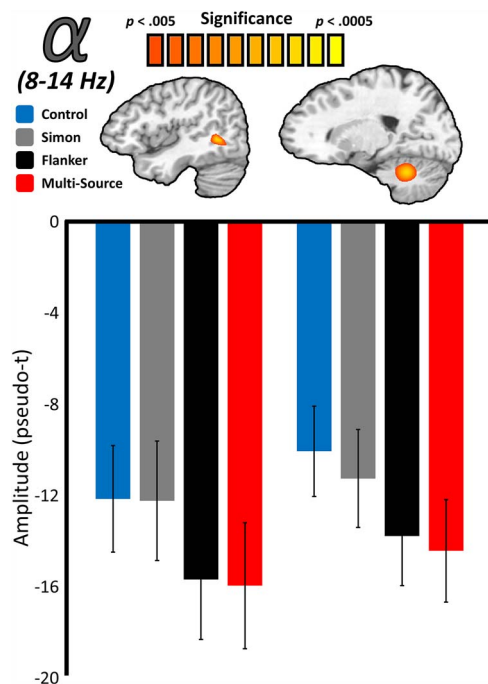


**Figure 4.** Main effects of interference on the posterior alpha response. Source-level images (top) reflect the significant results of whole-brain RM-ANOVAs testing for a main effect of interference condition on visual neural responses in the alpha-frequency (8–14 Hz) band, with the color scale bar at the top denoting voxel-wise significance. Below each image are the average response amplitude values (in pseudo-t) for each interference condition, with error bars denoting standard error of the mean (SEM). For both the right lateral occipital and right cerebellar peak voxels, responses to Simon interference did not differ from the control condition, and responses to Flanker interference did not differ from multisource interference. Responses to Simon and Flanker interference also significantly differed at both locations.

et al. 2011; Kujala et al. 2015; Wiesman 2015), with a long history of theories linking gamma activity to gamma-aminobutyric acid (GABA)-mediated local interneuronal circuits (Buzsáki and Wang 2012). In contrast, slower alpha-frequency rhythms are thought to be resultant of distal drives from the lateral geniculate and other areas of the thalamus (Andersen and Andersson 1968; da Silva 1991; Bollimunta et al. 2011).

In light of these previous findings on the role of alpha and gamma oscillations, the observed spectral double dissociation in the right lateral occipital cortices between interference subtypes provides critical insight. Essentially, stimulus–stimulus interference, such as that elicited by our Flanker and multisource (where both Flanker and Simon subtypes were present) interference conditions, would be expected to require a greater degree of active processing in higher order visual areas, since the source of the interference is external (i.e., flankers within the visual field) and would need to be actively parsed and suppressed. As discussed above, such external interference is likely mitigated by visual selective attention and related processes in the extended visual cortices, and this processing is widely believed to be indexed by decreases in alpha activity, which were robust in the right lateral occipital cortices for both the Flanker and multisource conditions. Conversely, in the control and Simon interference conditions, the nontarget stimuli (always 0) are not a source of interference, and thus less visual processing of these stimuli is needed for accurate performance, which

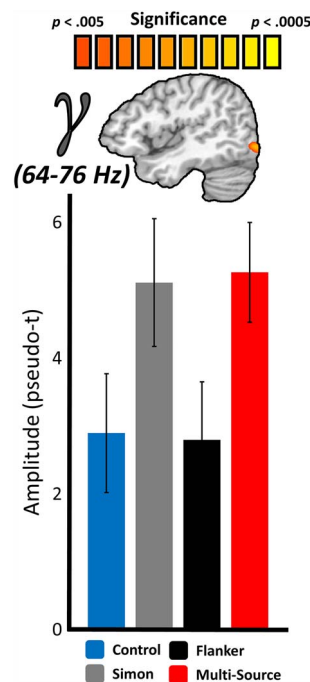


**Figure 5.** Main effects of interference on the posterior gamma response. Similar to Figure 3, the source-level image (top) represents the significant results of whole-brain RM-ANOVAs testing for a main effect of interference condition on neural responses in the gamma-frequency range (64–76 Hz), with the color scale bar at top denoting voxel-wise significance. Below the image are the average response amplitude values (in pseudo-t) for each interference condition, with error bars denoting SEM. For the right lateral occipital peak voxel, responses to Flanker interference did not differ from the control condition, and responses to Simon interference did not differ from multisource interference. Responses to Simon and Flanker interference also significantly differed at this location, as did responses to Flanker and multisource interference.

again is consistent with the much weaker alpha response in these two conditions relative to the Flanker and multisource. On the other hand, both the Simon and multisource conditions contain stimulus–response interference, whereby the prepotent motor responses (i.e., internal) are a primary source of interference. Thus, the critical processes include identifying the stimulus and rapid programming of the motor response. Such fine-grain coding of stimulus features and visuo-motor integration has been linked in previous research to gamma oscillations (Tallon-Baudry and Bertrand 1999; Bertrand and Tallon-Baudry 2000; Pesaran et al. 2002; Posada et al. 2003; Busch et al. 2004; Womelsdorf et al. 2006; Womelsdorf and Fries 2006; Van Der Werf et al. 2008; Muthukumaraswamy and Singh 2013). Once again, our primary MEG findings are consistent with this previous research, as we observed robust gamma oscillations in the right lateral occipital in the Simon and multisource, but not the Flanker and control conditions. Furthermore, our behavioral RT data also support the more rapid visual analyses and motor programming in the Simon relative to the Flanker condition.

The observed spectral double dissociation of cognitive interference subtypes in the lateral occipital cortices is noteworthy for at least two reasons. First, the vast majority of research regarding cognitive interference has focused on brain regions that are typically considered “higher order,” such as the prefrontal cortices (Hanslmayr et al. 2008; Zhu et al. 2010; Frühholz et al. 2011) and anterior cingulate cortex (Bush et al. 2003; Weissman et al. 2005; Hanslmayr et al. 2008; Frühholz et al. 2011;

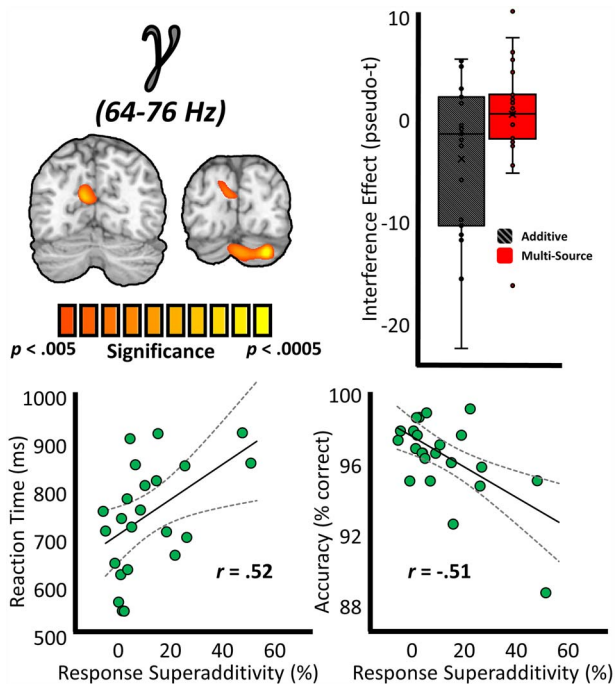


**Figure 6.** Superadditivity effects on the gamma response and relationships to behavior. (Top left) Source-level images on the left represent whole-brain paired-samples *t*-tests between the additive model (Flanker + Simon) and multisource model in the gamma band, with the color scale bar below denoting voxel-wise significance. (Top right) Box-and-whisker plot data demonstrating the superadditivity effect on gamma activity at the left superior parietal peak voxel. (Bottom) To examine the relationship between these neural indices and behavior, response superadditivity ( $[\text{multisource}/\text{additive}] \times 100$ ) values were computed for the superadditivity peaks, and these values were correlated with metrics of task performance. These relationships are displayed at the bottom, with RT (in ms) on the y-axis of the bottom left plot and accuracy (in % correct) denoted on the y-axis of the far right plot. For both plots, response superadditivity (in %) is denoted on the x-axis, and lines of best-fit are overlaid on the plot along with the correlation coefficient for each respective relationship.

Iannaccone et al. 2015). Thus, our findings are complementary to this past research and to an emerging line of research suggesting that cognitive interference has a robust effect at the level of late-stage visual processing (Gulbinaite et al. 2017; McDermott et al. 2017; Janssens et al. 2018), although our data go further in being the first to spectrally dissociate this late-stage visual processing effect based on the type of interference that is taking place. Second, a greater understanding of the spectral definitions of cognitive interference will certainly lend itself to future investigations on this topic. For example, the knowledge that lateral occipital gamma activity indexes stimulus–response interference, while alpha responses index stimulus–stimulus interference, could provide a starting point for noninvasive manipulations of these rhythms aimed at modulating human behavior. Rhythmic patterns of transcranial magnetic and electrical stimulation have already proven useful in a variety of contexts (Thut et al. 2011a, 2011b; Helfrich et al. 2014); however, to date no studies have attempted to modulate occipital dynamics in a spectrally specific manner with the ultimate goal of enhancing/degrading the impact of interference.

It should be noted that the spatial location of these effects (i.e., the “alpha-Flanker” and “gamma-Simon” clusters) was not perfectly overlapping, and in fact, the peak of the increased alpha-frequency responses to Flanker interference was slightly

more lateral and superior than the pattern of gamma responsiveness to Simon interference. This is in line with previous research as well; alpha-frequency activity is commonly found in “later” lateral occipital cortices, while gamma-frequency visual responses are commonly closer to “early” visual cortex. Importantly, this potential spatial distinction is an early clue that might also be useful in subsequent studies using spectrally- and spatially targeted stimulation of visual regions.

Although we did hypothesize that cognitive interference subtypes would exhibit unique effects on task performance and spectrally specific neural responses, we were surprised to also find a superadditive effect of multisource interference on these metrics. In studies of cognitive interference, superadditivity represents the inefficient handling of distinct cognitive processes by shared neural systems, and thus our behavioral data support that the neural systems indexing differing subtypes of cognitive interference overlap at least partially. Furthermore, we find that this overlap appears to reside in the superior parietal cortices spatially, and in the gamma-band spectrally. Previous findings of superadditive effects on cognitive processing in general have been in regard to different cognitive domains, including memory (Shimamura and Wickens 2009; Lwin et al. 2010), probability judgment (Macchi et al. 1999; Sloman et al. 2004), and multisensory integration (Holmes and Spence 2005; Laurienti et al. 2005), and so this finding was relatively unexpected. In terms of the underlying neurophysiology, superadditivity is typically reported in the form of increased neuronal spiking within a single cell or cell circuit (Holmes and Spence 2005); however, future research will be necessary to understand how this might relate to the frequency-specific increases in response to amplitude observed here.

Numerous studies have investigated potentially additive effects of stimulus–stimulus and stimulus–response subtypes on behavior, but the vast majority of them have found that the combined interference effects were subadditive. Although conflicting at first, our finding of superadditivity could be attributed to a number of discrepancies in experimental design and presentation. For instance, all previous studies known to us implemented the spatial conflict component of stimulus–response interference by presenting their entire stimulus set to the left or the right of fixation. While this manipulation certainly induces the intended interference effect in isolation, when combined with stimulus–stimulus interference, this presentation would almost certainly have influenced spatial attention. Furthermore, this presentation style only allowed for two potential responses susceptible to the stimulus–response interference (i.e., left or right presentation interfering with the right or left button press), and thus the stimulus–response interference load would have been substantially lower than in our design, where three potential responses were presented at one of three spatial locations. Although perhaps unlikely, it is possible that the greater interference load present in our study was necessary to tax shared neural resources to the point of exhibiting a negative effect on behavior. Finally, nearly all previous studies appear to have utilized a block design for presenting the different types of interfering stimuli, and such blocked designs are known to significantly affect the impact of cognitive interference on behavior (Stins et al. 2005). Regardless of the precise experimental discrepancies that these effects stem from, we found robust evidence of a superadditive effect of stimulus–stimulus and stimulus–response cognitive interference using an exceedingly simple adaptation of a well-studied cognitive paradigm. Future studies should vary some of

these experimental parameters to determine the critical players in superadditivity.

Interestingly, the superadditivity effect was observed not only in the task performance outcomes (i.e., RT and accuracy), but also in gamma-range neural responses in left superior parietal cortex and right cerebellum. The gamma-frequency superadditivity effect in left superior parietal cortex covaried robustly with RT and accuracy, signaling the task relevance of this response. While neural responses implicated in selective attention and cognitive control are often right lateralized (Thiebaut de Schotten et al. 2011; Aron et al. 2014), the recruitment of homologous cortices in the left hemisphere has been widely supported as being indicative of increased cognitive load (Reuter-Lorenz and Cappell 2008). Given this, it is then not surprising that our observed superadditivity effects were so tightly coupled to activity in the left superior parietal lobule, as a more distributed network of cortical nodes would be necessary to manage the increased disruption from simultaneously presented sources of interference.

Despite our novel findings, this research is not without its limitations. First, and perhaps most conspicuously, we did not observe any significant conditional effects in the anterior cingulate cortex, which has been reported in previous fMRI studies of the MSIT (Bush et al. 2003; Bush and Shin 2006). One potential explanation for this null finding is again the differences in experiment presentation, and in particular, the blocked design (Stins et al. 2005). Additionally, MEG is more sensitive to superficial sources of neural activity, and so it is possible that cingulate activity was present, but not as easily resolved by our measurement and/or statistical methods. Second, while this task design allows for extremely effective balancing of visual stimuli across interference subtypes, it does not allow for perfect balancing of the number of stimulus sets within each condition. This equates to three stimulus sets for the control condition, six stimulus sets for the Simon and Flanker conditions, and twelve stimulus sets for the multisource condition. While this certainly raises questions of a confounding effect of novelty, our results do not appear to reflect this potential effect. The induced amplitude in the alpha and gamma bands was selectively increased in the Flanker and Simon conditions, respectively, and these increases were both present in the multisource condition. In the case of the superadditivity effect in the left superior parietal cortices, there was no significant difference in this response among the control, Simon, and Flanker conditions—only between these three conditions and the multisource condition. Thus, it appears that these data did not follow the “novelty pattern” that would be expected (i.e., control < Flanker = Simon < multisource). It should also be noted that the correct response required was evenly balanced across the four conditions (i.e., an equal ratio of index, middle, and ring-finger responses). Third, exploratory analyses investigating phase-phase and phase-amplitude relationships between the lateral occipital and superior parietal regions identified in this manuscript did not suggest significant coupling. While it is potentially the case that no such coupling exists, it is equally likely that limitations inherent to this dataset precluded us from finding any connectivity that does exist, and future studies should further examine this potential. Finally, the potential involvement of motor responses (i.e., the beta desynchronization and gamma synchronization) in these effects was not within the (already broad) scope of this study. Future research should certainly focus on this aspect, particularly in light of recent reports of interference effects

in the motor cortex (Gaetz et al. 2013; Heinrichs-Graham et al. 2018). Despite these limitations, these findings are of interest, as they shine new light on the spectral-, temporal, and spatial-properties of cognitive interference in the human brain. A number of patient populations suffer from an inability to appropriately manage cognitive interference, including but not limited to Alzheimer’s disease (Baddeley et al. 2001), diabetes (Embury et al. 2018), human immunodeficiency virus (HIV)-associated neurocognitive disorders (Lew et al. 2018), schizophrenia (McGhie 1964), attention deficit (Bush et al. 2008), and amyotrophic lateral sclerosis (Vieregge et al. 1999; Pinkhardt et al. 2008). Hopefully, the findings from this study can be used to further both basic research into the neural underpinnings of these disorders, as well as translational research into potential therapeutics (e.g., transcranial stimulation to enhance cognitive performance).

## Supplementary Material

Supplementary material is available at *Cerebral Cortex* online.

## Funding

National Institutes of Health (grants R01-MH103220 to T.W.W., R01-MH116782 to T.W.W., R01-MH118013 to T.W.W., and F31-AG055332 to A.I.W.); National Science Foundation (grant #1539067 to T.W.W.); NASA Nebraska Space Grant (A.I.W.).

## Notes

The funders had no role in study design, data collection and analysis, decision to publish, or preparation of the manuscript. *Conflict of Interest:* The authors declare no competing interests, financial or otherwise.

## References

- Andersen P, Andersson SA. 1968. *Physiological basis of the alpha rhythm*. New York: Plenum Publishing Corporation.
- Aron AR, Robbins TW, Poldrack RA. 2004. Inhibition and the right inferior frontal cortex. *Trends Cogn Sci*. 8(4):170–177.
- Aron AR, Robbins TW, Poldrack RA. 2014. Inhibition and the right inferior frontal cortex: one decade on. *Trends Cogn Sci*. 18(4):177–185.
- Baayen RH, Milin P. 2010. Analyzing reaction times. *Int J Psychol Res*. 3(2):12–28.
- Baddeley AD, Baddeley HA, Bucks RS, Wilcock GK. 2001. Attentional control in alzheimer’s disease. *Brain*. 124(Pt 8): 1492–1508.
- Başar E, Başar-Eroglu C, Karakas S, Schürmann M. 2001. Gamma, alpha, delta, and theta oscillations govern cognitive processes. *Int J Psychophysiol*. 39(2–3):241–248.
- Bertrand O, Tallon-Baudry C. 2000. Oscillatory gamma activity in humans: a possible role for object representation. *Int J Psychophysiol*. 38(3):211–223.
- Bisley JW, Goldberg ME. 2010. Attention, intention, and priority in the parietal lobe. *Annu Rev Neurosci*. 33:1–21.
- Bollimunta A, Mo J, Schroeder CE, Ding M. 2011. Neuronal mechanisms and attentional modulation of corticothalamic alpha oscillations. *Journal of Neuroscience*. 31(13):4935–4943.

- Bonnefond M, Jensen O. 2012. Alpha oscillations serve to protect working memory maintenance against anticipated distracters. *Curr Biol.* 22(20):1969–1974.
- Brainard DH. 1997. The psychophysics toolbox. *Spatial Vision.* 10:433–436.
- Bush NA, Debener S, Kranczioch C, Engel AK, Herrmann CS. 2004. Size matters: effects of stimulus size, duration and eccentricity on the visual gamma-band response. *Clin Neurophysiol.* 115(8):1810–1820.
- Buschman TJ, Miller EK. 2007. Top-down versus bottom-up control of attention in the prefrontal and posterior parietal cortices. *Science.* 315(5820):1860–1862.
- Bush G, Shin LM. 2006. The multi-source interference task: an fMRI task that reliably activates the cingulo-frontal-parietal cognitive/attention network. *Nat Protoc.* 1(1):308–313.
- Bush G, Shin LM, Holmes J, Rosen BR, Vogt BA. 2003. The multi-source interference task: validation study with fMRI in individual subjects. *Mol Psychiatry.* 8(1):60–70.
- Bush G, Spencer TJ, Holmes J, Shin LM, Valera EM, Seidman LJ, Makris N, Surman C, Aleari M, Mick E. 2008. Functional magnetic resonance imaging of methylphenidate and placebo in attention-deficit/hyperactivity disorder during the multi-source interference task. *Archives of General Psychiatry.* 65(1):102–114.
- Buzsáki G, Wang X-J. 2012. Mechanisms of gamma oscillations. *Annual review of neuroscience.* 35:203–225.
- Capotosto P, Babiloni C, Romani GL, Corbetta M. 2009. Frontoparietal cortex controls spatial attention through modulation of anticipatory alpha rhythms. *J Neurosci.* 29(18):5863–5872.
- Colby CL, Goldberg ME. 1999. Space and attention in parietal cortex. *Annu Rev Neurosci.* 22:319–349.
- Corbetta M, Shulman GL, Miezin FM, Petersen SE. 1995. Superior parietal cortex activation during spatial attention shifts and visual feature conjunction. *Science.* 270(5237):802–805.
- da Silva FL. 1991. Neural mechanisms underlying brain waves: from neural membranes to networks. *Electroencephalography and clinical neurophysiology.* 79(2):81–93.
- de Graaf TA, Gross J, Paterson G, Rusch T, Sack AT, Thut G. 2013. Alpha-band rhythms in visual task performance: phase-locking by rhythmic sensory stimulation. *PLoS One.* 8(3):e60035.
- Desmurget M, Epstein CM, Turner RS, Prablanc C, Alexander GE, Grafton ST. 1999. Role of the posterior parietal cortex in updating reaching movements to a visual target. *Nat Neurosci.* 2(6):563–567.
- Doesburg SM, Bedo N, Ward LM. 2016. Top-down alpha oscillatory network interactions during visuospatial attention orienting. *Neuroimage.* 132:512–519.
- Doesburg SM, Roggeveen AB, Kitajo K, Ward LM. 2008. Large-scale gamma-band phase synchronization and selective attention. *Cereb Cortex.* 18(2):386–396.
- Edden RA, Muthukumaraswamy SD, Freeman TC, Singh KD. 2009. Orientation discrimination performance is predicted by GABA concentration and gamma oscillation frequency in human primary visual cortex. *J Neurosci.* 29(50):15721–15726.
- Embury CM, Wiesman AI, McDermott TJ, Proskovec AL, Heinrichs-Graham E, Lord GH, Brau KL, Drincic AT, Desouza CV, Wilson TW. 2018. The impact of type 1 diabetes on neural activity serving attention. *Hum Brain Mapp.*
- Ergen M, Saban S, Kirmizi-Alsan E, Uslu A, Keskin-Ergen Y, Demiralp T. 2014. Time-frequency analysis of the event-related potentials associated with the stroop test. *Int J Psychophysiol.* 94(3):463–472.
- Eriksen BA, Eriksen CW. 1974. Effects of noise letters upon the identification of a target letter in a nonsearch task. *Percept Psychophys.* 16(1):143–149.
- Ernst MD. 2004. Permutation methods: a basis for exact inference. *Statistical Sci.* 19(4):676–685.
- Fox MD, Corbetta M, Snyder AZ, Vincent JL, Raichle ME. 2006. Spontaneous neuronal activity distinguishes human dorsal and ventral attention systems. *Proc Natl Acad Sci USA.* 103(26):10046–10051.
- Foxe JJ, Snyder AC. 2011. The role of alpha-band brain oscillations as a sensory suppression mechanism during selective attention. *Front Psychol.* 2:154.
- Frühholz S, Godde B, Finke M, Herrmann M. 2011. Spatiotemporal brain dynamics in a combined stimulus-stimulus and stimulus-response conflict task. *Neuroimage.* 54(1):622–634.
- Gaetz W, Edgar JC, Wang DJ, Roberts TP. 2011. Relating MEG measured motor cortical oscillations to resting  $\gamma$ -aminobutyric acid (GABA) concentration. *Neuroimage.* 55(2):616–621.
- Gaetz W, Liu C, Zhu H, Bloy L, Roberts TP. 2013. Evidence for a motor gamma-band network governing response interference. *Neuroimage.* 74:245–253.
- Gross J, Kujala J, Hamalainen M, Timmermann L, Schnitzler A, Salmelin R. 2001. Dynamic imaging of coherent sources: studying neural interactions in the human brain. *Proc Natl Acad Sci USA.* 98(2):694–699.
- Gruber T, Müller MM, Keil A, Elbert T. 1999. Selective visual-spatial attention alters induced gamma band responses in the human EEG. *Clin Neurophysiol.* 110(12):2074–2085.
- Gulbinaite R, van Viegen T, Wieling M, Cohen MX, VanRullen R. 2017. Individual alpha peak frequency predicts 10 Hz flicker effects on selective attention. *J Neurosci.* 37(42):10173–10184.
- Hampshire A, Chamberlain SR, Monti MM, Duncan J, Owen AM. 2010. The role of the right inferior frontal gyrus: inhibition and attentional control. *Neuroimage.* 50(3):1313–1319.
- Handel BF, Haarmeier T, Jensen O. 2011. Alpha oscillations correlate with the successful inhibition of unattended stimuli. *J Cogn Neurosci.* 23(9):2494–2502.
- Hanslmayr S, Pastötter B, Bäuml KH, Gruber S, Wimber M, Klimesch W. 2008. The electrophysiological dynamics of interference during the stroop task. *J Cogn Neurosci.* 20(2):215–225.
- He BJ, Snyder AZ, Vincent JL, Epstein A, Shulman GL, Corbetta M. 2007. Breakdown of functional connectivity in frontoparietal networks underlies behavioral deficits in spatial neglect. *Neuron.* 53(6):905–918.
- Heinrichs-Graham E, Hoburg JM, Wilson TW. 2018. The peak frequency of motor-related gamma oscillations is modulated by response competition. *Neuroimage.* 165:27–34.
- Heinrichs-Graham E, Wilson TW. 2015. Spatiotemporal oscillatory dynamics during the encoding and maintenance phases of a visual working memory task. *Cortex.* 69:121–130.
- Helfrich RF, Schneider TR, Rach S, Trautmann-Lengsfeld SA, Engel AK, Herrmann CS. 2014. Entrainment of brain oscillations by transcranial alternating current stimulation. *Curr Biol.* 24(3):333–339.
- Herring JD, Thut G, Jensen O, Bergmann TO. 2015. Attention modulates tms-locked alpha oscillations in the visual cortex. *J Neurosci.* 35(43):14435–14447.



- Holliday IE, Barnes GR, Hillebrand A, Singh KD. 2003. Accuracy and applications of group MEG studies using cortical source locations estimated from participants' scalp surfaces. *Hum Brain Mapp.* 20(3):142–147.
- Holmes NP, Spence C. 2005. Multisensory integration: space, time and superadditivity. *Current Biol.* 15(18):R762–R764.
- Iannaccone R, Hauser TU, Staempfli P, Walitza S, Brandeis D, Brem S. 2015. Conflict monitoring and error processing: new insights from simultaneous EEG-fMRI. *Neuroimage.* 105:395–407.
- Janssens C, De Loof E, Boehler CN, Pourtois G, Verguts T. 2018. Occipital alpha power reveals fast attentional inhibition of incongruent distractors. *Psychophysiology.* 55(3):e13011.
- JASP-Team. 2018. Jasp (version 0.8.3.1).
- Jensen O, Gips B, Bergmann TO, Bonnefond M. 2014. Temporal coding organized by coupled alpha and gamma oscillations prioritize visual processing. *Trends Neurosci.* 37(7):357–369.
- Jensen O, Kaiser J, Lachaux JP. 2007. Human gamma-frequency oscillations associated with attention and memory. *Trends Neurosci.* 30(7):317–324.
- Jensen O, Mazaheri A. 2010. Shaping functional architecture by oscillatory alpha activity: gating by inhibition. *Front Hum Neurosci.* 4:186.
- Kelly SP, Lalor EC, Reilly RB, Foxe JJ. 2006. Increases in alpha oscillatory power reflect an active retinotopic mechanism for distracter suppression during sustained visuospatial attention. *J Neurophysiol.* 95(6):3844–3851.
- Klimesch W. 2012. A-band oscillations, attention, and controlled access to stored information. *Trends Cogn Sci.* 16(12):606–617.
- Koelewijn L, Rich AN, Muthukumaraswamy SD, Singh KD. 2013. Spatial attention increases high-frequency gamma synchronisation in human medial visual cortex. *Neuroimage.* 79:295–303.
- Kovach CK, Gander PE. 2016. The demodulated band transform. *J Neurosci Methods.* 261:135–154.
- Kriegeskorte N, Simmons WK, Bellgowan PS, Baker CI. 2009. Circular analysis in systems neuroscience: the dangers of double dipping. *Nat Neurosci.* 12(5):535–540.
- Kujala J, Jung J, Bouvard S, Lecaigard F, Lothe A, Bouet R, Ciomas C, Ryvlin P, Jerbi K. 2015. Gamma oscillations in v1 are correlated with GABA(a) receptor density: a multi-modal MEG and flumazenil-pet study. *Sci Rep.* 5:16347.
- Landau AN, Schreyer HM, van Pelt S, Fries P. 2015. Distributed attention is implemented through theta-rhythmic gamma modulation. *Curr Biol.* 25(17):2332–2337.
- Laurienti PJ, Perrault TJ, Stanford TR, Wallace MT, Stein BE. 2005. On the use of superadditivity as a metric for characterizing multisensory integration in functional neuroimaging studies. *Experimental Brain Research.* 166(3–4):289–297.
- Lew BJ, McDermott TJ, Wiesman AI, O'Neill J, Mills MS, Robertson KR, Fox HS, Swindells S, Wilson TW. 2018. Neural dynamics of selective attention deficits in HIV-associated neurocognitive disorder. *Neurology.* 91(20):e1860–e1869.
- Liu X, Banich MT, Jacobson BL, Tanabe JL. 2004. Common and distinct neural substrates of attentional control in an integrated Simon and spatial stroop task as assessed by event-related fMRI. *Neuroimage.* 22(3):1097–1106.
- Lwin MO, Morrin M, Krishna A. 2010. Exploring the superadditive effects of scent and pictures on verbal recall: an extension of dual coding theory. *Journal of Consumer Psychology.* 20(3):317–326.
- Lynch JC, Mountcastle VB, Talbot WH, Yin TC. 1977. Parietal lobe mechanisms for directed visual attention. *J Neurophysiol.* 40(2):362–389.
- Macchi L, Osherson D, Krantz DH. 1999. A note on superadditive probability judgment. *Psychological Review.* 106(1):210.
- Maris E, Oostenveld R. 2007. Nonparametric statistical testing of EEG- and MEG-data. *J Neurosci Methods.* 164(1):177–190.
- Marshall TR, O'Shea J, Jensen O, Bergmann TO. 2015. Frontal eye fields control attentional modulation of alpha and gamma oscillations in contralateral occipitoparietal cortex. *J Neurosci.* 35(4):1638–1647.
- May ES, Butz M, Kahlbrock N, Hoogenboom N, Brenner M, Schnitzler A. 2012. Pre- and post-stimulus alpha activity shows differential modulation with spatial attention during the processing of pain. *Neuroimage.* 62(3):1965–1974.
- McDermott TJ, Wiesman AI, Mills MS, Spooner RK, Coolidge NM, Proskovec AL, Heinrichs-Graham E, Wilson TW. 2019. Tdcs modulates behavioral performance and the neural oscillatory dynamics serving visual selective attention. *Hum Brain Mapp.* 40(3):729–740.
- McDermott TJ, Wiesman AI, Proskovec AL, Heinrichs-Graham E, Wilson TW. 2017. Spatiotemporal oscillatory dynamics of visual selective attention during a flanker task. *Neuroimage.* 156:277–285.
- McGhie A. 1964. Disturbances in selective attention in schizophrenia. *Proc R Soc Med.* 57:419–422.
- Mountcastle VB, Lynch JC, Georgopoulos A, Sakata H, Acuna C. 1975. Posterior parietal association cortex of the monkey: command functions for operations within extrapersonal space. *J Neurophysiol.* 38(4):871–908.
- Muthukumaraswamy SD, Edden RA, Jones DK, Swettenham JB, Singh KD. 2009. Resting GABA concentration predicts peak gamma frequency and fMRI amplitude in response to visual stimulation in humans. *Proc Natl Acad Sci USA.* 106(20):8356–8361.
- Muthukumaraswamy SD, Singh KD. 2013. Visual gamma oscillations: the effects of stimulus type, visual field coverage and stimulus motion on MEG and EEG recordings. *Neuroimage.* 69:223–230.
- Nombela C, Nombela M, Castell P, García T, López-Coronado J, Herrero MT. 2014. Alpha-theta effects associated with ageing during the stroop test. *PLoS One.* 9(5):e95657.
- Pesaran B, Pezaris JS, Sahani M, Mitra PP, Andersen RA. 2002. Temporal structure in neuronal activity during working memory in macaque parietal cortex. *Nat Neurosci.* 5(8):805–811.
- Peterson BS, Kane MJ, Alexander GM, Lacadie C, Skudlarski P, Leung HC, May J, Gore JC. 2002. An event-related functional MRI study comparing interference effects in the Simon and Stroop tasks. *Brain Res Cogn Brain Res.* 13(3):427–440.
- Pinkhardt EH, Jürgens R, Becker W, Mölle M, Born J, Ludolph AC, Schreiber H. 2008. Signs of impaired selective attention in patients with amyotrophic lateral sclerosis. *J Neurol.* 255(4):532–538.
- Poline JB, Worsley KJ, Holmes AP, Frackowiak RS, Friston KJ. 1995. Estimating smoothness in statistical parametric maps: variability of p values. *J Comput Assist Tomogr.* 19(5):788–796.
- Posada A, Hugues E, Franck N, Vianin P, Kilner J. 2003. Augmentation of induced visual gamma activity by increased task complexity. *Eur J Neurosci.* 18(8):2351–2356.

- Posner MI, Walker JA, Friedrich FJ, Rafal RD. 1984. Effects of parietal injury on covert orienting of attention. *J Neurosci.* 4(7):1863–1874.
- Reuter-Lorenz PA, Cappell KA. 2008. Neurocognitive aging and the compensation hypothesis. *Curr Dir Psychol Sci.* 17(3):177–182.
- Rihs TA, Michel CM, Thut G. 2007. Mechanisms of selective inhibition in visual spatial attention are indexed by alpha-band EEG synchronization. *Eur J Neurosci.* 25(2):603–610.
- Rohenkohl G, Nobre AC. 2011. A oscillations related to anticipatory attention follow temporal expectations. *J Neurosci.* 31(40):14076–14084.
- Romei V, Gross J, Thut G. 2010. On the role of prestimulus alpha rhythms over occipito-parietal areas in visual input regulation: correlation or causation? *J Neurosci.* 30(25):8692–8697.
- Shibata T, Shimoyama I, Ito T, Abia D, Iwasa H, Koseki K, Yamanouchi N, Sato T, Nakajima Y. 1999. Attention changes the peak latency of the visual gamma-band oscillation of the EEG. *Neuroreport.* 10(6):1167–1170.
- Shimamura AP, Wickens TD. 2009. Superadditive memory strength for item and source recognition: the role of hierarchical relational binding in the medial temporal lobe. *Psychol Rev.* 116(1):1.
- Siegel M, Donner TH, Oostenveld R, Fries P, Engel AK. 2007. High-frequency activity in human visual cortex is modulated by visual motion strength. *Cereb Cortex.* 17(3):732–741.
- Simon JR. 1990. The effects of an irrelevant directional cue on human information processing. *Advances in psychology.* Amsterdam: Elsevier. p. 31–86.
- Sloman S, Rottenstreich Y, Wisniewski E, Hadjichristidis C, Fox CR. 2004. Typical versus atypical unpacking and superadditive probability judgment. *J Exp Psychol Learn Mem Cogn.* 30(3):573.
- Spaak E, de Lange FP, Jensen O. 2014. Local entrainment of alpha oscillations by visual stimuli causes cyclic modulation of perception. *J Neurosci.* 34(10):3536–3544.
- Stins JF, van Leeuwen WM, de Geus EJ. 2005. The multi-source interference task: the effect of randomization. *J Clin Exp Neuropsychol.* 27(6):711–717.
- Suzuki K, Okumura Y, Kita Y, Oi Y, Shinoda H, Inagaki M. 2018. The relationship between the superior frontal cortex and alpha oscillation in a flanker task: simultaneous recording of electroencephalogram (EEG) and near infrared spectroscopy (nirs). *Neurosci Res.* 131:30–35.
- Tallon-Baudry C, Bertrand O. 1999. Oscillatory gamma activity in humans and its role in object representation. *Trends Cogn Sci.* 3(4):151–162.
- Tallon-Baudry C, Bertrand O, Henaff MA, Isnard J, Fischer C. 2005. Attention modulates gamma-band oscillations differently in the human lateral occipital cortex and fusiform gyrus. *Cereb Cortex.* 15(5):654–662.
- Taulu S, Simola J. 2006. Spatiotemporal signal space separation method for rejecting nearby interference in MEG measurements. *Phys Med Biol.* 51(7):1759–1768.
- Thiebaut de Schotten M, Dell'Acqua F, Forkel SJ, Simmons A, Vergani F, Murphy DG, Catani M. 2011. A lateralized brain network for visuospatial attention. *Nat Neurosci.* 14(10):1245–1246.
- Thut G, Schyns PG, Gross J. 2011a. Entrainment of perceptually relevant brain oscillations by non-invasive rhythmic stimulation of the human brain. *Front Psychol.* 2:170.
- Thut G, Veniero D, Romei V, Miniussi C, Schyns P, Gross J. 2011b. Rhythmic tms causes local entrainment of natural oscillatory signatures. *Curr Biol.* 21(14):1176–1185.
- Tiesinga P, Sejnowski TJ. 2009. Cortical enlightenment: are attentional gamma oscillations driven by ping or pong? *Neuron.* 63(6):727–732.
- Uhlhaas PJ, Pipa G, Neuenschwander S, Wibral M, Singer W. 2011. A new look at gamma? High- (>60 Hz)  $\gamma$ -band activity in cortical networks: function, mechanisms and impairment. *Prog Biophys Mol Biol.* 105(1–2):14–28.
- Uusitalo MA, Ilmoniemi RJ. 1997. Signal-space projection method for separating MEG or EEG into components. *Med Biol Eng Comput.* 35(2):135–140.
- Van Der Werf J, Jensen O, Fries P, Medendorp WP. 2008. Gamma-band activity in human posterior parietal cortex encodes the motor goal during delayed prosaccades and antisaccades. *J Neurosci.* 28(34):8397–8405.
- van Dijk H, Schoffelen JM, Oostenveld R, Jensen O. 2008. Prestimulus oscillatory activity in the alpha band predicts visual discrimination ability. *J Neurosci.* 28(8):1816–1823.
- van Veen V, Carter CS. 2002. The anterior cingulate as a conflict monitor: fMRI and ERP studies. *Physiol Behav.* 77(4–5):477–482.
- Verbruggen F, Aron AR, Stevens MA, Chambers CD. 2010. Theta burst stimulation dissociates attention and action updating in human inferior frontal cortex. *Proc Natl Acad Sci USA.* 107(31):13966–13971.
- Vidal JR, Chaumon M, O'Regan JK, Tallon-Baudry C. 2006. Visual grouping and the focusing of attention induce gamma-band oscillations at different frequencies in human magnetoencephalogram signals. *J Cogn Neurosci.* 18(11):1850–1862.
- Viergege P, Wauschkuhn B, Heberlein I, Hagenah J, Verleger R. 1999. Selective attention is impaired in amyotrophic lateral sclerosis—a study of event-related EEG potentials. *Brain Res Cogn Brain Res.* 8(1):27–35.
- Wang K, Li Q, Zheng Y, Wang H, Liu X. 2014. Temporal and spectral profiles of stimulus-stimulus and stimulus-response conflict processing. *Neuroimage.* 89:280–288.
- Weissman DH, Gopalakrishnan A, Hazlett CJ, Woldorff MG. 2005. Dorsal anterior cingulate cortex resolves conflict from distracting stimuli by boosting attention toward relevant events. *Cereb Cortex.* 15(2):229–237.
- Wiesman AI, Wilson TW. 2019. Alpha Frequency Entrainment Reduces the Effect of Visual Distractors. *J Cogn Neurosci.* 31(9):1392–1403.
- Wiesman AI, Rezich MT, O'Neill J, Morsey B, Wang T, Ideker T, Swindells S, Fox HS, Wilson TW. 2019. Epigenetic Markers of Aging Predict the Neural Oscillations Serving Selective Attention. *Cereb Cortex.* (epub).
- West R, Bell MA. 1997. Stroop color-word interference and electroencephalogram activation: evidence for age-related decline of the anterior attention system. *Neuropsychology.* 11(3):421–427.
- Wiesman AI. 2015. Homotypic synaptic coupling and the cellular bases of gamma oscillatory activity. *Journal of neurophysiology.* 115(2):625–627.
- Wiesman AI, Heinrichs-Graham E, McDermott TJ, Santamaria PM, Gendelman HE, Wilson TW. 2016. Quiet connections: reduced fronto-temporal connectivity in nondemented parkinson's disease during working memory encoding. *Hum Brain Mapp.*

- Wiesman AI, Heinrichs-Graham E, Proskovec AL, McDermott TJ, Wilson TW. 2017. Oscillations during observations: dynamic oscillatory networks serving visuospatial attention. *Hum Brain Mapp.* 38(10):5128–5140.
- Wiesman AI, Mills MS, McDermott TJ, Spooner RK, Coolidge NM, Wilson TW. 2018a. Polarity-dependent modulation of multi-spectral neuronal activity by transcranial direct current stimulation. *Cortex.* 108:222–233.
- Wiesman AI, O'Neill J, Mills MS, Robertson KR, Fox HS, Swindells S, Wilson TW. 2018b. Aberrant occipital dynamics differentiate HIV-infected patients with and without cognitive impairment. *Brain.*
- Womelsdorf T, Fries P. 2006. Neuronal coherence during selective attentional processing and sensory-motor integration. *J Physiol Paris.* 100(4):182–193.
- Womelsdorf T, Fries P, Mitra PP, Desimone R. 2006. Gamma-band synchronization in visual cortex predicts speed of change detection. *Nature.* 439(7077):733–736.
- Worden MS, Foxe JJ, Wang N, Simpson GV. 2000. Anticipatory biasing of visuospatial attention indexed by retinotopically specific alpha-band electroencephalography increases over occipital cortex. *J Neurosci.* 20(6):RC63.
- Worsley KJ, Andermann M, Koulis T, MacDonald D, Evans AC. 1999. Detecting changes in nonisotropic images. *Hum Brain Mapp.* 8(2–3):98–101.
- Worsley KJ, Marrett S, Neelin P, Vandal AC, Friston KJ, Evans AC. 1996. A unified statistical approach for determining significant signals in images of cerebral activation. *Hum Brain Mapp.* 4(1):58–73.
- Yantis S, Schwarzbach J, Serences JT, Carlson RL, Steinmetz MA, Pekar JJ, Courtney SM. 2002. Transient neural activity in human parietal cortex during spatial attention shifts. *Nat Neurosci.* 5(10):995–1002.
- Zhu DC, Zacks RT, Slade JM. 2010. Brain activation during interference resolution in young and older adults: an fMRI study. *Neuroimage.* 50(2):810–817.